

# Seismic Performance of Flange Plate Connections to Built-up Box Columns

**A. Deylami, M. Tehranizadeh & M. Gholami**

*Amirkabir University of Technology, Iran*



## SUMMARY

This paper presents analytical and experimental studies on the cyclic behavior of flange plate connection between a steel beam and a welded box column. Three full-scale specimens were tested to evaluate the effect of flange plate length and plate-to-flange fillet weld geometry on the seismic response of flange plate connection. Flange plate connection in the test specimens achieved the AISC seismic provision requirements for special moment frames. Then, the finite-element model developed using ABAQUS was validated using the test results. This model was subsequently used to further investigate the behavior of the test specimens.

*keywords: Connections; Flange Plate; Box Columns; Experimental program; Finite element analysis*

## 1. INTRODUCTION

Box columns are frequently employed in areas of high seismic risk because they have an excellent capacity to resist biaxial bending. Cold-formed hollow sections are often used for low and medium rise buildings and built-up sections made up of four plates welded together are used for high rise buildings (Nakashima et al, 2000). Extensive studies have been carried out and several new connection details have been proposed for the connection of I-beams to wide flange columns since the 1994 Northridge earthquake (Kim et al, 2002, Ricles et al, 2002, Chen et al, 2005, Tabar et al, 2004, Shiravand et al, 2010, Adeli et al, 2011). But limited research for the connection of I-beams to box-columns has been conducted (Chen et al, 2004). Kim et al. (2004) tested two full-scale moment connections to US box columns fabricated using pre-Northridge connection details. Test results revealed that both specimens failed by brittle fracture of complete joint penetration (CJP) welds between the beam flange and the column during a story drift angle of less than 1% rad, which resulted in no plastic rotation in the connections. Chen et al (2004) tested six large scale specimens of steel beam-to-box column connections. One of the test specimens was the unreinforced connection using pre-Northridge details, and other test specimens were the reinforced connections using rib plates or wing plates. The unreinforced connection was failed by fracture in the heat affected zone (HAZ) of the beam bottom flange during 2.3% story drift angle cycle.

In the present study the behavior of welded flange plate (WFP) connection, shown in Fig. 1, has been investigated. The geometry of these plates is considered in a manner that site welding in a horizontal position is possible for connecting flange plates to beam and column. In this study, three full-scale specimens were tested to evaluate the effect of flange plate length and plate-to-flange fillet weld geometry on the seismic response of flange plate connection. Then, a validated finite element model was used to further investigate local response in flange plate connections.

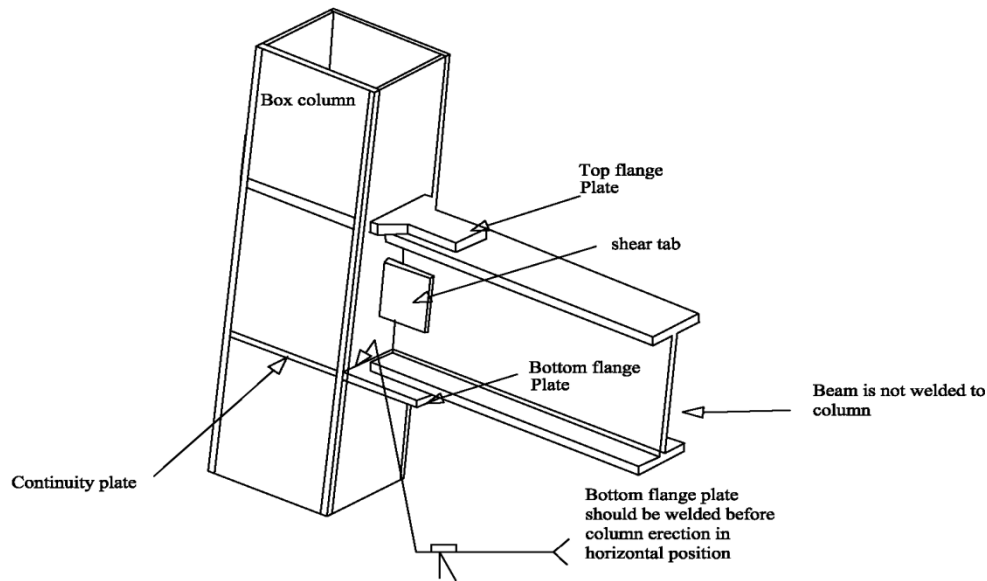


**Figure 1.** Field welded moment connection.

## 2. EXPERIMENTAL PROGRAM

The behavior of the moment connections under severe cyclic loading, particularly in regard to the initiation and propagation of fracture, cannot be reliably predicted by analytical means alone. Consequently, the satisfactory performance of connections must be confirmed by laboratory testing (AISC-341, 2005). Therefore, an experiment was carried out to clarify the seismic behavior of the flange plate connections. The testing procedure and test results for global and local seismic behavior of the test specimens are presented in the following sections.

### 2.1. Test specimens

A total of three large-scale specimens were designed to simulate an exterior T-shaped joint subassembly. Each subassembly contained a column between the mid-height of the two adjacent floors and a half-span of the beam. The general configuration of the subassembly is shown in Fig. 2. The joint from the steel beam to the box column was a flange plate moment connection. All specimens were constructed with a I-380 × 200 × 8 × 12 (mm) beam and a built-up B-400 × 400 × 20 × 20 (mm) box column, to reduce the influence of the size of the beam and the column on the connection behavior. Summary information on the specimens is presented in Table 2.1. Fig. 3 shows connection details of specimen LF30. In the specimen LF30, flange plates were joined to the beam flanges with longitudinal fillet welds only. Specimen LF50 was identical to LF30 except that the flange-plate length was increased from 300 to 500 mm. Specimen LF50-T was similar to specimen LF50 except for the addition of the transverse fillet weld at the nose of the flange plate; the size of the LF50-T fillet welds was smaller than that of LF50 to preserve the total volume of fillet weld material. Fig. 4 is a plan view of the fillet welds joining the beam flange to the flange plate in specimens LF50 and LF50-T.

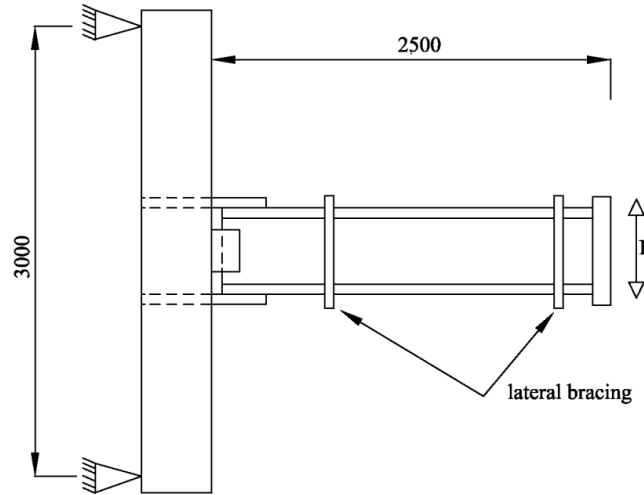


**Figure 2.** Configuration of the exterior joint subassembly

**Table 2.1.** Summary Information on specimens

specimen	Connection type	Flange-plate length	Top flange-plate thickness	Bottom flange-plate thickness	Longitudinal fillet weld	Transverse fillet weld
LF30	Flange plate	300	20	15	10	-----
LF50	Flange plate	500	25	20	10	-----
LF50-T	Flange plate	500	25	20	8	8

Note: All dimensions in mm.

## 2.2. Test setup and instrumentation

According to the shape of the specimens, a test setup was prepared to simulate the boundary conditions of the exterior joint subassembly in a laterally loaded moment frame. The column top and bottom were supported by real hinges. The beam was laterally braced in the vicinity of the plastic hinge and also near the beam end. The general configuration of the test setup is shown in Fig. 5. The cyclic displacement proposed by AISC seismic provisions was applied at the tip of the beam by a hydraulic actuator

## 2.3. General test observations

Figs. 6, 7 and 8 show the test specimens LF30, LF50 and LF50-T at the end of the test, respectively. For all the specimens, plastic hinge forms in the beam at the nose of flange plate. Such a result is desirable because the objective of the flange-plate connection is to force inelastic action in the beam away from the column face. In the specimens LF50 and LF50-T, tearing was occurred at the groove weld joining the beam web to the beam flange in the plastic hinge location, as shown in Fig. 8. In contrast, no crack was observed in the specimen LF30. This result indicates that a longer flange plate can lead to a greater potential for fracture at the plastic hinge location. Fig. 9 shows the tearing in the beam flange at the end of the longitudinal fillet weld of specimens LF50 and LF30. In the specimen LF50-T, the transverse fillet weld prevented the tearing in the beam at the nose of flange plate.

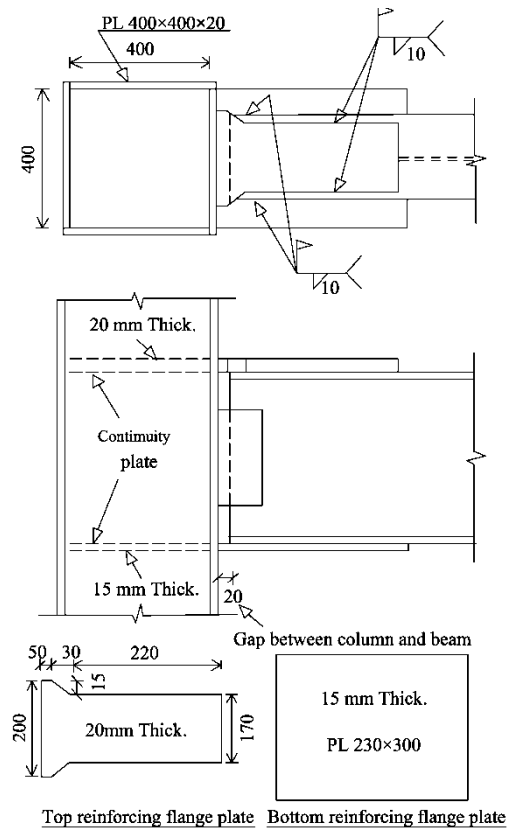


**Figure 3.** Connection details of specimen LF30

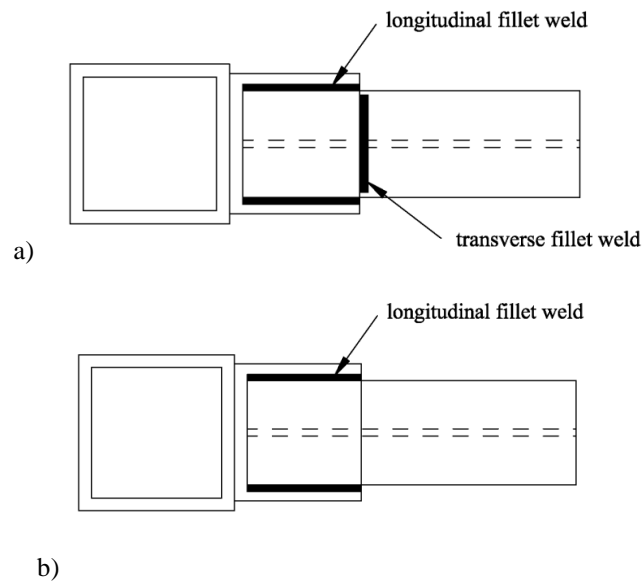


**Figure 4.** Fillet weld geometry: ( a) LF50-T and (b) LF50



**Figure 5.** Test setup configuration



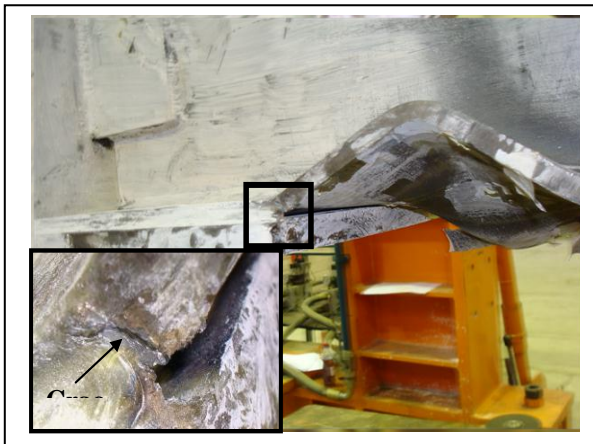
**Figure 6.** Specimen LF30 at the end of the test



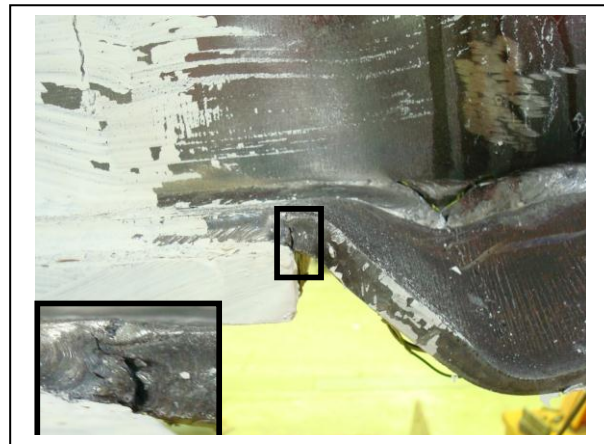
**Figure 7.** Specimen LF50 at the end of the test



**Figure 8.** Specimen LF50-T at the end of the test



a)



b)

**Figure 9.** Tearing in the beam flange at the end of the longitudinal fillet weld of specimens a) LF30 and b) LF50

**2.4. General evaluation of the connection behavior**

The hysteretic curves of the moment at the column face versus story drift angle ( $\theta$ ) for test specimens LF30 and LF50 are presented in Fig. 10. The story drift angle is computed by dividing the total beam tip displacement by the distance from the beam tip to the column centerline. The hysteretic curve of specimen LF50-T was similar to that of specimen LF50. In all the specimens, moment resistance at 4% total story drift was more than 80% plastic moment of beam. Therefore, flange plate connection in all the specimens achieved the AISC seismic provision requirements for special moment frames. It should be noted that the strength degradation of the specimens resulted from ductile local and global buckles during the cyclic loading.

In order to have a good comparison between the hysteretic curves of the specimens LF50 and LF30 a combined plot is illustrated in Fig. 11. This figure shows that LF50-T and LF50 dissipated more energy than LF30. The reason for this result is that a longer flange plate increase distance from the column face to plastic hinge, and consequently increase flexural moment at the beam-to-column interface.

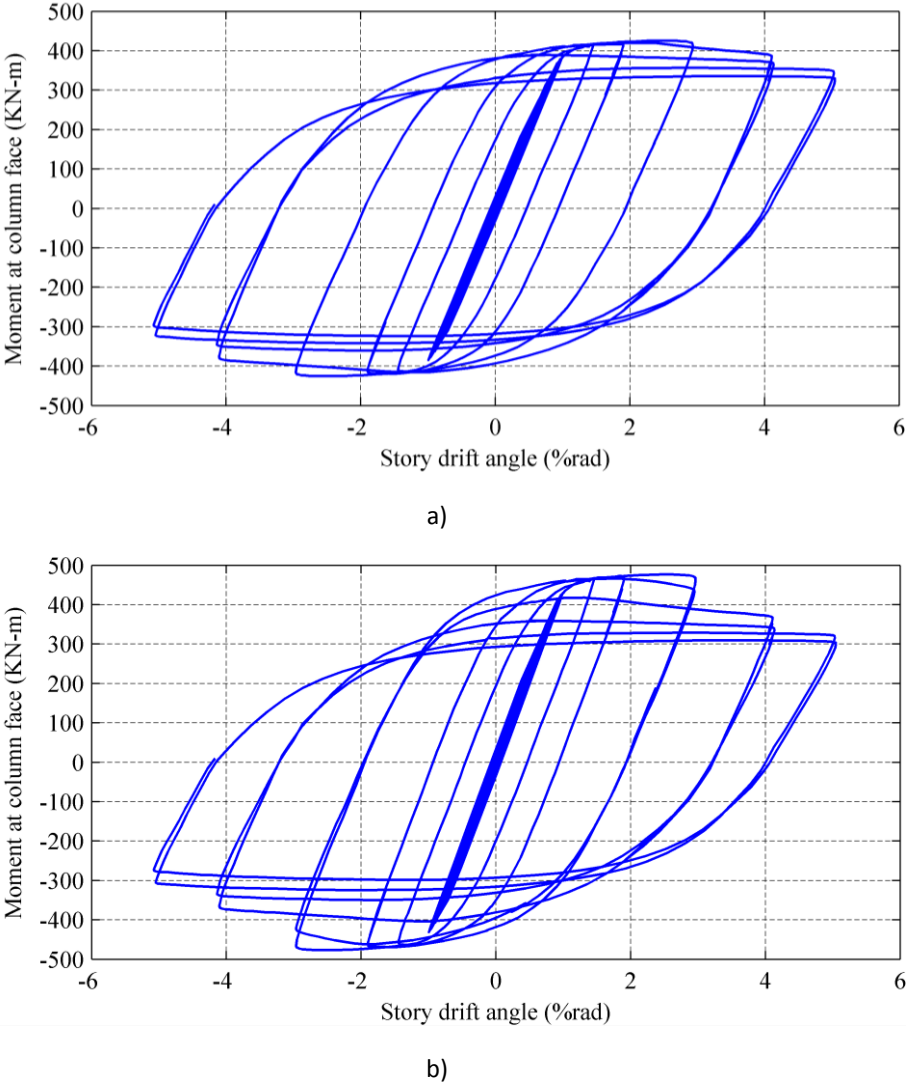


**Figure 10.** The hysteretic curves for test specimens a) LF30 and b) LF50

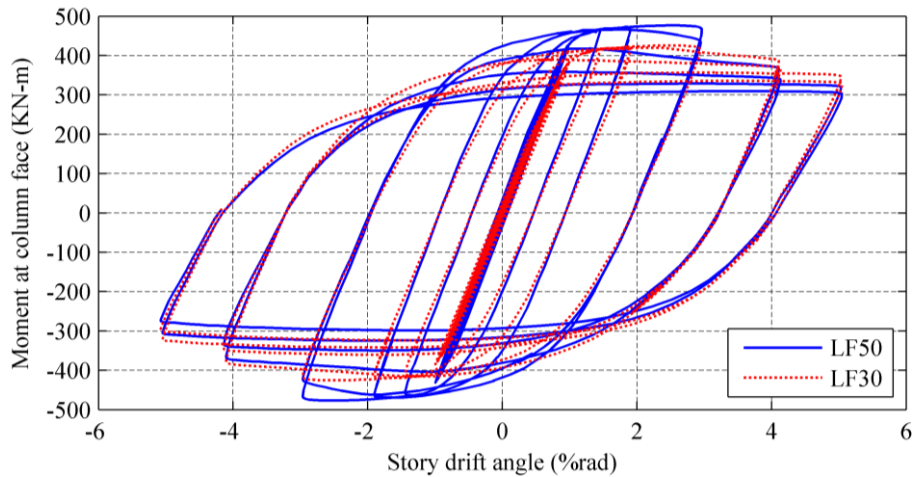


**Figure 11.** Comparison between the hysteretic curves of the test specimens LF50 and LF30

### 3. NONLINEAR FINITE ELEMENT ANALYSIS

#### 3.1. Finite element modeling

As shown in Fig. 12, groove welds and fillet welds were modeled. The beam, column, plates, CJP groove welds and fillet welds in the model were discretized using three-dimensional solid (brick) elements. The size of the finite-element mesh varied over the length and height of the model. A fine-mesh was used near the connection of the beam to the column and the beam flange to the reinforcing plate. A coarser mesh was used elsewhere. Most of the solid elements were right-angle prisms. Hinged boundary conditions were used to support the column top and bottom.

Data from tests of coupons extracted from the beam and column of specimen were used to establish the stress-strain relationships for the beam and column elements. The weld material was modeled using the test data of Kaufmann (1997). Table 3.1 presents the material properties used for the analytical models. A bilinear stress-strain relationship was assumed for each of the components identified in Table 3.1. The Poisson's ratio was taken as 0.3 for all materials throughout the analyses. To account for material nonlinearities, the von mises yield criterion was employed.

**Table 3.1.** Material properties

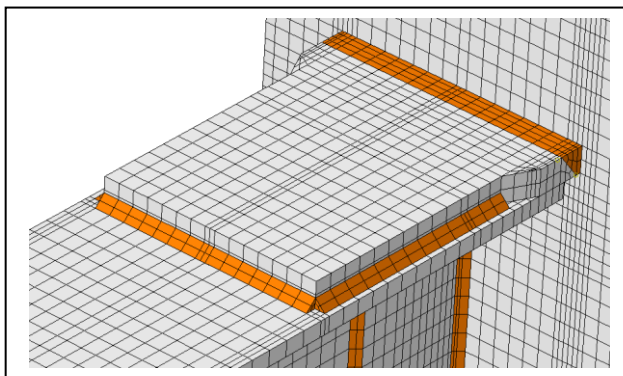


**Figure 12.** Finite element model

Material	Yield point		Ultimate point	
	$\sigma_y$	$\epsilon_y$	$\sigma_u$	$\epsilon_u$
Steel	3000	0.15	4200	18
Weld	5200	0.26	5600	12

#### 3.2. Model validation

The finite element analysis of specimens LF30, LF50 and LF50-T were performed. The cyclic outcomes are compared with the cyclic experimental results in Fig. 13. As shown, the experimental and finite element results are in good agreement. While the ultimate load and initial stiffness are well

evaluated, the extant differences between the two data sets are justified by geometric differences between the finite element models and specimens, uncertainties in the material model, and also unavoidable residual stresses.

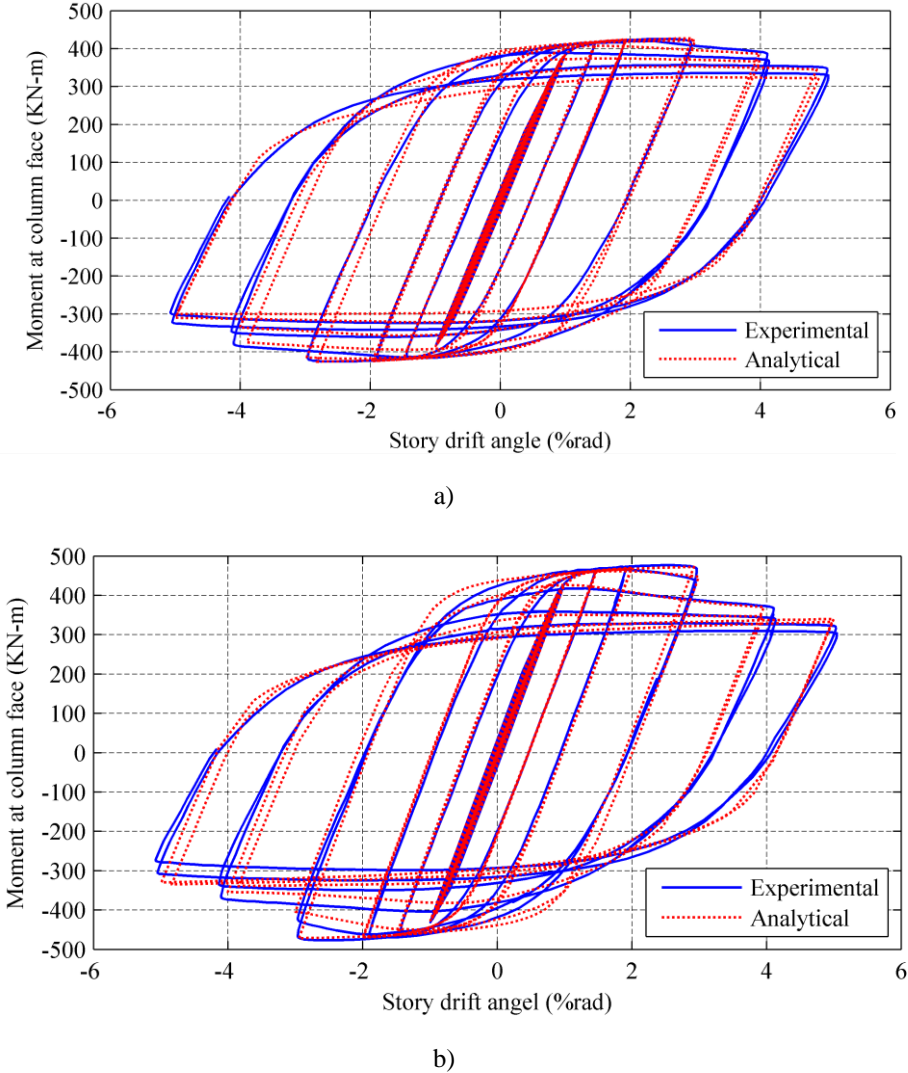
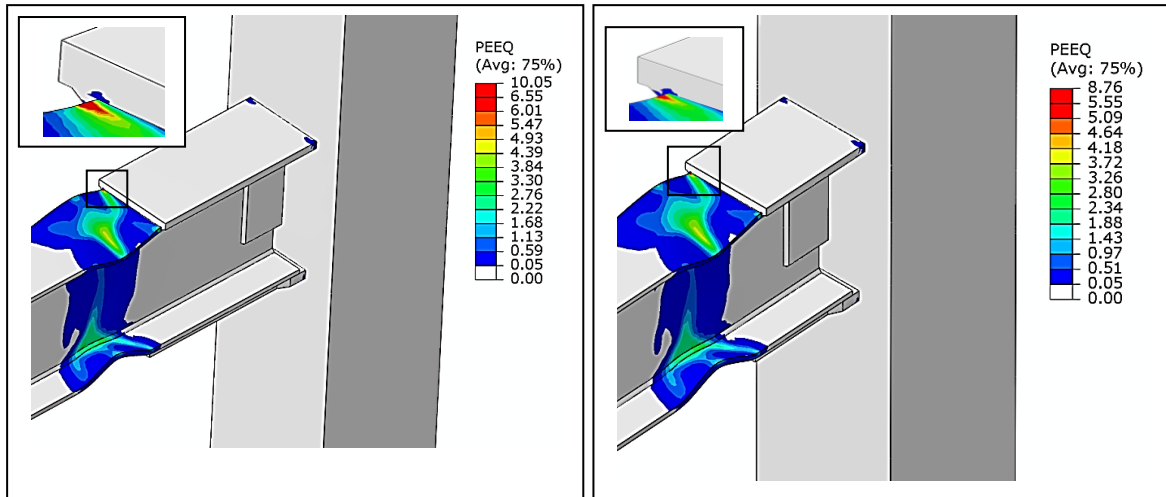


**Figure 13.** Combined plot of experimental and analytical results for specimens a) LF30 and b) LF50

**3.3. PEEQ distribution in finite element models**

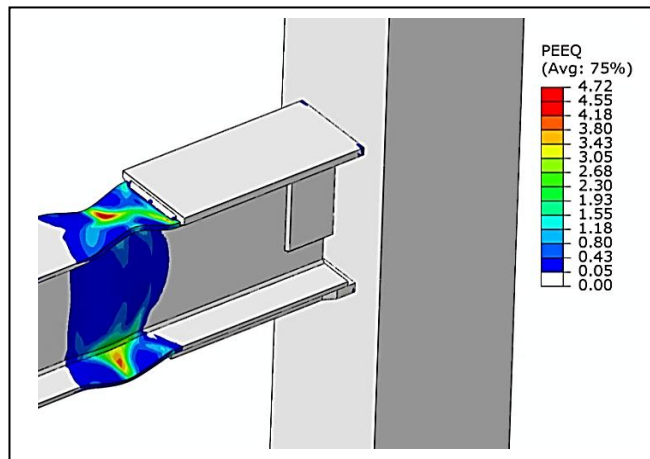
Fig. 14 presents the PEEQ contours in the finite element models LF30, LF50 and LF50-T. The key observations from Fig. 18 are 1) finite element models exhibited behavior as observed in the test specimens in the way of forming plastic hinge in the beam at the nose of flange plates, 2) strain concentration was occurred at the end of the longitudinal fillet weld of specimens LF30 and LF50. This highly strained regions in the analytical models correspond to the location of the cracks observed in the test specimens LF30 and LF50 3) the addition of the transverse fillet weld in LF50-T prevented the strain concentration at the end of the longitudinal fillet weld. For this reason, no crack was observed at the nose of flange plate of test specimen LF50-T.

Fig. 15 presents the PEEQ contours in the groove weld joining the beam web to the beam flange at the plastic hinge region for models LF30 and LF50. This Figure indicates that a longer flange plate increase PEEQ value in the groove weld joining the beam web to the beam flange at the plastic hinge region. For this reason, the tearing was occurred in the groove weld at the plastic hinge region of specimens LF50 and LF50-T.



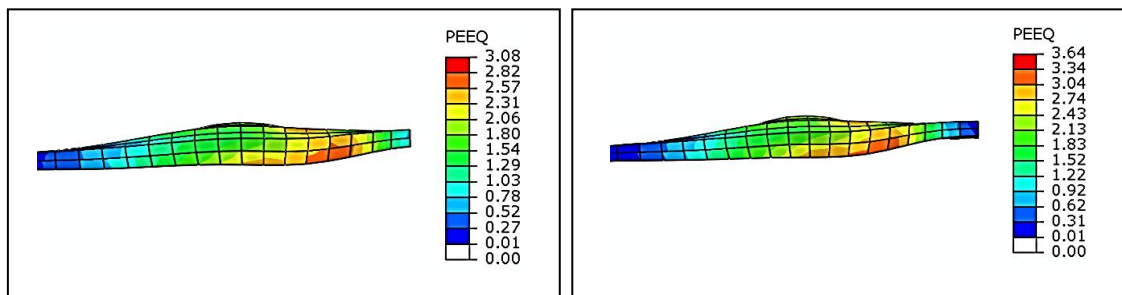
a)

b)



c)

**Figure 14.** Equivalent plastic strain distribution in the finite element models a) LF50, b) L30 and c) LF50-T



a)

b)

**Figure 15.** Equivalent plastic strain distribution in the groove weld joining the beam web to the beam flange

at the plastic hinge region for models a) LF30 and b) LF50

#### 4. CONCLUSION

Three full-scale specimens with flange plate connections were tested to evaluate the effect of flange plate length and plate-to-beam flange fillet weld geometry on the seismic response of connection. Each specimen composed of a I-shaped steel beam with the dimensions of I-380×200×8×12 (mm) connected to a box column with the measurements of B-400 × 400 × 20 × 20 (mm). Flange plate connection in the test specimens achieved the AISC seismic provision requirements for special moment frames. Then, a validated finite element model was used to further investigate local response in flange plate connections.

The key conclusions drawn from the analytical studies and the associated experimental results are:

1. In the flange plate connections, plastic hinge forms in the beam at the nose of flange plate. For this reason no damage was observed at the groove welds joining flange plates to column flange.
2. The addition of the transverse fillet weld at the nose of flange plate will reduces PEEQ value at the end of longitudinal fillet welds and consequently prevents the tearing in the beam at the end of the longitudinal fillet welds.
3. In the specimens with longer flange plate, tearing was occurred in the groove weld joining the beam web to the beam flange at the plastic hinge region because use of a longer flange plate increases PEEQ value in the groove weld at the plastic hinge region.

#### REFERENCES

- Nakashima, M., Roeder, CW. and Maruoka, Y. (2000). Steel moment frames for earthquakes in United States and Japan. *J Struct Eng* **126:8**, 861–8.
- Kim T., Whittaker AS., Gilani ASJ., Bertero VV. and Takhirov SM. (2002). Cover-plate and flange-plate steel moment-resisting connections. *Journal of Structural Engineering* **128:4**, 474–482.
- Ricles JM., Fisher JW., Lu LW. and Kaufmann EJ. (2002). Development of improved welded moment connections for earthquake-resistant design. *Journal of Constructional Steel Research* **58:4**, 565–604.
- Chen CC., Chen SW., Chung MD. and Lin MC. (2005). Cyclic behavior of unreinforced and rib-reinforced moment connections. *Journal of Constructional Steel Research* **61:6**, 1–21.
- Tabar, A.M. and Deylami, A. (2004). Investigation of major parameters affecting instability of steel beams with RBS moment connections. *Steel and Composite Structures* **6:3**, 1475-1491.
- Shiravand, M. and Deylami, A. (2010). Application of Full Depth Side Plate to Moment Connection of I-Beam to Double-I Column. *Advances in Structural Engineering* **13:6**, 1047-1062.
- Adeli, M., Banazadeh, M. and Deylami, A. (2011). Bayesian approach for determination of drift hazard curves for generic steel moment-resisting frames in territory of Tehran. *International Journal of Civil Engineering* **9: 3**, 145-154.
- Chen CC., Lin CC. and Tsai CL. (2004). Evaluation of reinforced connections between steel beams and box columns. *Engineering Structures* **13:5**, 1089–1092.
- Kim T, Whittaker AS, Gilani ASJ, Bertero VV, Takhirov SM, Ostertag C, 2002 ”, Forensic studies of a large cover plat steel moment resisting connection” *The Structural Design of Tall Buildings* 11, 265–283.
- Kaufmann, E. J. (1997). Dynamic tension tests of simulated moment resisting frame weld joints. Chicago. Steel Tips, Structural Steel Education Council, *American Institute of Steel Construction* .